

Supplementary Material for the article
“ Alternation between planar and coiled modes in slender rods
embedded in soft elastic matrices”

Tianxiang Su^{a,†}, Jia Liu^{a,†}, Denis Terwagne^{b,c,†}, Pedro M. Reis^{*,b,d}, and Katia Bertoldi^{*,a,e}

^a*School of Engineering and Applied Sciences, Harvard University, Cambridge, MA, 02138, USA*

^b*Department of Civil and Environmental Engineering, Massachusetts Institute of Technology, Cambridge, MA, 02139, USA*

^c*Current address: Faculté des Sciences, Université Libre de Bruxelles (ULB), Bruxelles 1050, Belgium*

^d*Department of Mechanical Engineering, Massachusetts Institute of Technology, Cambridge, MA, 02139, USA*

^e*Kavli Institute for Bionano Science and Technology, Harvard University, Cambridge, MA, 02138, USA*

[†]*These authors contributed equally to this work.*

^{*}*To whom correspondence may be addressed. E-mail: preis@mit.edu and bertoldi@seas.harvard.edu*

S1 Experiment setup

Fabricating matrices with different stiffness

For the fabrication of the elastomeric matrix surrounding the Nitinol rod, we used PDMS (Sylgard 184 from Dow Corning Inc.). This product comes in two parts, a curing agent and a base agent, that we have to mix prior curing. Curing of the PDMS was performed using a convection oven at a low temperature of $T = 40^\circ \text{C}$ for 24 hours ensuring a negligible thermal dilatation of the molds and PDMS and thus stress free samples after curing. The Dow Corning recommendation is to use a base/cure ratio in weight of 10:1, which produce an elastomer of Young modulus of 2100 kPa after curing. By varying the base/cure ratio from 80:1 to 10:1 and thus changing the amount of cross linkers, one can vary the Young modulus of the elastomeric sample, typically from 1 kPa to 2.1 MPa.

To measure the elastic modulus, we casted a small cylinder sample (2 cm long and 2.6 cm in diameter) along with each PDMS matrix using the same mixture and protocol. These small cylinders were then tested under compression using a Zwick material testing machine. By importing the displacement and force measurements and using a linear elastic model, we deduced the Young modulus for each of the elastomeric matrices. Due to the geometry of our test, i.e. the barreling of the sample cylinder when compressed, a correction factor on the inferred Young modulus had to be taken into account [1]. These measurements of the elastic modulus as a function of ratio base/cure agent are represented on Fig. S1 along with other results taken from the literature [2, 3, 4, 5].

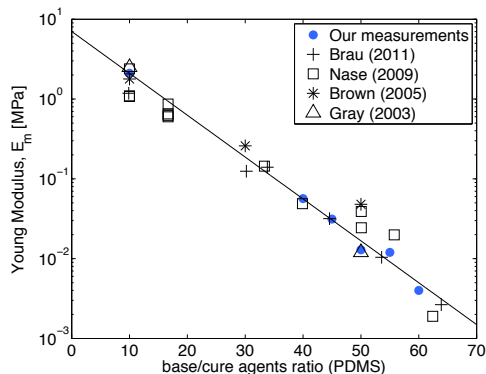
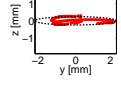
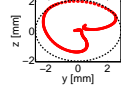
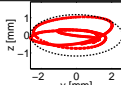
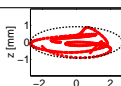
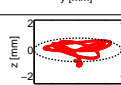
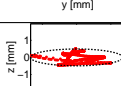
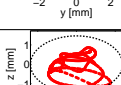
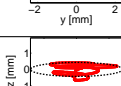
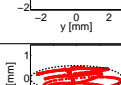
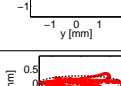
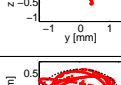
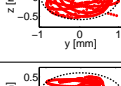
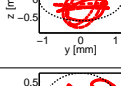
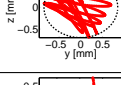
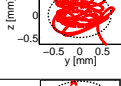


Figure S1: Elastic modulus of Polydimethylsiloxane Dow Corning Sylgard 184 as a function of the ratio of base agent on cure agent. Measurements on our samples are represented using full disk symbol along with other measurements from the literature [2, 3, 4, 5].

Sample parameters

We made a total of 15 samples in this study. The parameters for all the samples and their cross-sectional buckling shapes at compressive strain $\epsilon = 3\%$ are shown in Tab. S1.

Table S1: Parameters characterizing all the 15 samples. d_r is diameter of the rod; E_r is the Young's modulus of the rod; E_m is the Young's modulus of the matrix; L_r is the length of the rod; δ_{\max} is the maximum applied displacement during the test; $E_m L_r^4 / (E_r I_r)$ is the dimensionless matrix stiffness, $I_r = \pi d_r^4 / 64$ being the second moment of inertia of the rod cross section. In the last column a cross sectional view of the buckled sample at $\epsilon = 3\%$ is shown.

| Name | d_r [μm] | E_r [GPa] | E_m [kPa] | L_r [m] | δ_{\max} [mm] | $E_m L_r^4 / E_r I_r$ [10^6] | Buckled shape $\epsilon = 3\%$ |
|------|----------------------------|------------------|------------------|--------------|-------------------------|-------------------------------------|---|
| S26 | 203 | 59.23 ± 0.07 | 32.59 ± 0.69 | 0.041 | 2 | 0.0190 |  |
| S25 | 254 | 67.01 ± 0.69 | 32.59 ± 0.69 | 0.055 | 2.5 | 0.0213 |  |
| S15 | 254 | 67.01 ± 0.69 | 29.45 ± 0.50 | 0.097 | 4 | 0.19 |  |
| S24 | 203 | 59.23 ± 0.07 | 13.85 ± 0.33 | 0.098 | 5 | 0.26 |  |
| S8 | 254 | 67.01 ± 0.69 | 66.73 ± 0.96 | 0.099 | 5 | 0.47 |  |
| S17 | 203 | 59.23 ± 0.07 | 32.85 ± 0.54 | 0.097 | 3 | 0.59 |  |
| S23 | 152 | 67.95 ± 0.77 | 13.85 ± 0.33 | 0.097 | 7 | 0.69 |  |
| S21 | 203 | 59.23 ± 0.07 | 49.63 ± 0.67 | 0.097 | 4 | 0.89 |  |
| S14 | 152 | 67.95 ± 0.77 | 29.45 ± 0.50 | 0.097 | 4 | 1.46 |  |
| S7 | 152 | 67.95 ± 0.77 | 59.96 ± 0.78 | 0.094 | 4 | 2.63 |  |
| S22 | 100 | 64.24 ± 0.24 | 13.85 ± 0.33 | 0.097 | 9 | 3.89 |  |
| S16 | 100 | 64.24 ± 0.24 | 32.85 ± 0.54 | 0.097 | 9 | 9.22 |  |
| S20 | 100 | 64.24 ± 0.24 | 49.63 ± 0.67 | 0.097 | 6 | 13.93 |  |
| S18 | 50.8 | 60.93 ± 1.26 | 10.05 ± 0.32 | 0.097 | 5 | 44.68 |  |
| S13 | 50.8 | 60.93 ± 1.26 | 29.45 ± 0.50 | 0.097 | 5 | 130.87 |  |

S2 Computing the minimum area ellipse that encloses the cross-sectional view of the buckled rod

To better characterize the buckling shape, for each sample we computed the minimum area ellipse that encloses the cross-sectional view of the buckled rod at a given level of applied compressive strain ϵ . First, to facilitate the analysis, we rigidly rotated the rod using Principal Component Analysis (PCA) [6, 7] and aligned the major lateral buckling direction with the y axis (the matrix central axis was aligned with x). Then, we focused on the lateral $y - z$ plane and computed the ellipse with the smallest possible area that encloses all points $[y_i, z_i]$ along the rod (note that to eliminate boundary effects, we only focused on points of the rod away from the boundaries and neglected those within 1/6 of its length from both ends). Therefore, denoting with a and b the major and minor axes of the ellipse, we required

$$\frac{y_i^2}{a^2} + \frac{z_i^2}{b^2} \leq 1, \quad \text{for all } i = 1, 2, 3, \dots, N \quad (\text{S1})$$

so that

$$a^2 \geq \max_i \left(\frac{y_i^2}{1 - z_i^2/b^2} \right). \quad (\text{S2})$$

Therefore, for a given a value of b the lower bound for the area of the ellipse $S = \pi a b$ was obtained as

$$S = \pi a b \geq \max_i \left(\frac{\pi y_i}{\sqrt{1/b^2 - z_i^2/b^4}} \right). \quad (\text{S3})$$

Finally, we determined numerically the minor axis b that minimizes the area,

$$S_{\min} = \min_b \left[\max_i \left(\frac{\pi y_i}{\sqrt{1/b^2 - z_i^2/b^4}} \right) \right]. \quad (\text{S4})$$

Two examples of minimum area ellipses (black dashed line) obtained for samples #7 and #18 together with the trace of rod coordinates (red line) are shown in Fig. S2A and B. Note that the aspect ratio of the ellipse (*i.e.*, the ratio between the minor and major axes b/a) characterizes whether the buckling shape is 2D or 3D: A flat ellipse with a small b/a value indicates an in-plane buckling shape, while a more circular one with $b/a \rightarrow 1$ indicates a 3D buckling shape.

S3 Buckling analysis using the Winkler foundation model

While in the main text we focus on the results of the buckling analysis, here we present the details of the analysis.

To understand and quantify the conditions leading to 2D and 3D buckling configurations, we adopt the Winkler foundation model and simplify the matrix as an array of springs with stiffness K acting only in radial direction. Consequently, assuming small strain and moderate rotation, the governing equation for the embedded elastic rod is given by

$$E_r I_r \frac{\partial^4 Y}{\partial S^4} + F \frac{\partial^2 Y}{\partial S^2} + K Y = 0, \quad (\text{S5})$$

where $E_r I_r$ is the bending stiffness of the rod, F is the applied compressive force and Y and S denote the lateral displacement and the arc length of the rod, respectively. By introducing

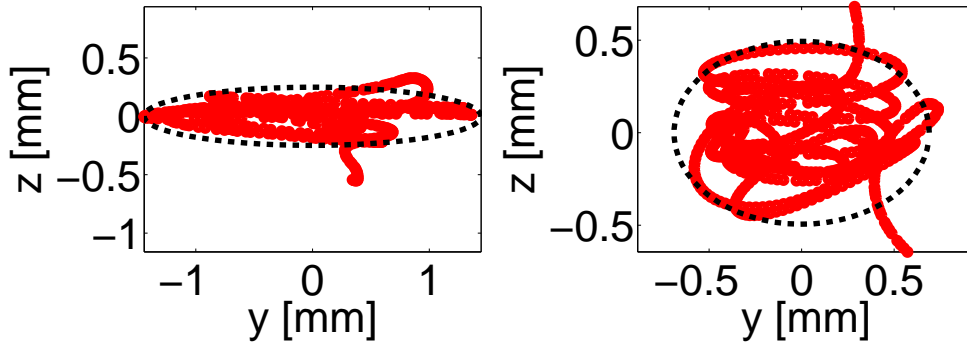


Figure S2: Two examples of minimum area ellipses (dashed black lines) that enclose the cross-sectional view of the buckled rod (red traces).

the normalized displacement, $y = Y/L_r$, and arc length, $s = S/L_r$, Eq. (S5) can be rewritten in dimensionless form as

$$\frac{\partial^4 y}{\partial s^4} + \pi^2 f \frac{\partial^2 y}{\partial s^2} + \pi^4 k y = 0, \quad (\text{S6})$$

where $f = FL_r^2/(\pi^2 E_r I_r)$ and $k = KL_r^4/(\pi^4 E_r I_r)$ are the dimensionless compressive force and spring constant, respectively.

To solve for the critical force f_{cr} , one needs to specify boundary conditions. Here, we consider two types of boundary conditions: (*Case A*) both ends are free to rotate; (*Case B*) both ends are fixed.

Case A: Both ends are free-to-rotate

When both ends of the rod are free to rotate,

$$y(0) = y(1) = 0, \quad y''(0) = y''(1) = 0 \quad (\text{S7})$$

where $(\cdot)' = \partial(\cdot)/\partial s$. For this case, the solution of Eq. (S6) takes the form

$$y(s) = A \sin(n\pi s), \quad (\text{S8})$$

where n is an integer. Substitution of Eq. (S8) into Eq. (S6) yields

$$A n^4 \pi^4 \sin(n\pi s) - A n^2 \pi^4 f \sin(n\pi s) + A \pi^4 k \sin(n\pi s) = 0, \quad (\text{S9})$$

which can be simplified as

$$n^4 - n^2 f + k = 0. \quad (\text{S10})$$

Therefore, non-trivial solutions to Eq. (S6) exist when

$$f = f_n = \frac{k + n^4}{n^2}, \quad (\text{S11})$$

where f_n denotes the compressive force f_n required to trigger the n -th mode. Since during loading the mode associated to the lowest f_n emerges and grows, the critical buckling force for the system is given by

$$f_{cr} = \min_{n=1,2,\dots} \left(n^2 + \frac{k}{n^2} \right). \quad (\text{S12})$$

Case B: both ends are fixed

When both ends of the rod are fixed

$$y(0) = y(1) = 0, \quad y'(0) = y'(1) = 0, \quad (\text{S13})$$

and the form of solution to Eq. (S6) is found by examining the roots of its characteristic equation

$$x^4 + \pi^2 f x^2 + \pi^4 k = 0. \quad (\text{S14})$$

Note that the form of the solution depends on the sign of $f^2 - 4k$.

1. For $f^2 - 4k > 0$, Eq. (S14) has four imaginary roots,

$$\alpha = \pm \frac{i\pi}{\sqrt{2}} \sqrt{f + \sqrt{f^2 - 4k}}, \quad \beta = \pm \frac{i\pi}{\sqrt{2}} \sqrt{f - \sqrt{f^2 - 4k}}. \quad (\text{S15})$$

Therefore, the general solution to Eq. (S6) is given by

$$y(s) = A_1 \sin(\alpha s) + A_2 \cos(\alpha s) + A_3 \sin(\beta s) + A_4 \cos(\beta s), \quad (\text{S16})$$

so that

$$y'(s) = A_1 \alpha \cos(\alpha s) - A_2 \alpha \sin(\alpha s) + A_3 \beta \cos(\beta s) - A_4 \beta \sin(\beta s) \quad (\text{S17})$$

where A_1, A_2, A_3, A_4 are arbitrary constants which are determined by imposing the boundary conditions. Substitution of Eqs. (S16) and (S17) into the boundary conditions (S13), yields

$$\begin{aligned} A_2 + A_4 &= 0 \\ A_1 \alpha + A_3 \beta &= 0 \\ A_1 \sin(\alpha) + A_2 \cos(\alpha) + A_3 \sin(\beta) + A_4 \cos(\beta) &= 0 \\ A_1 \alpha \cos(\alpha) - A_2 \alpha \sin(\alpha) + A_3 \beta \cos(\beta) - A_4 \beta \sin(\beta) &= 0 \end{aligned} \quad (\text{S18})$$

which can be written as $\mathbf{K}\mathbf{a} = \mathbf{0}$, where \mathbf{K} is a coefficient matrix and $\mathbf{a} = (A_1, A_2, A_3, A_4)^T$. Generally, the matrix \mathbf{K} is not singular and only the trivial solution $\mathbf{a} = \mathbf{0}$ exists. However, for certain values of f , \mathbf{K} becomes singular (i.e. $\det(\mathbf{K}) = 0$) and in that case a non-zero solution is found, indicating the occurrence of buckling. Note that in this case explicit formulae for the critical force cannot be obtained and buckling is detected numerically by finding the values of f for which $\det(\mathbf{K}) = 0$.

2. If $f^2 - 4k = 0$, the roots of Eq. (S14) are given by

$$\alpha = \pm i \pi k^{1/4}, \quad (\text{S19})$$

and the solution of Eq. (S6) takes the form

$$y(s) = A_1 \sin(\alpha s) + A_2 s \sin(\alpha s) + A_3 \cos(\alpha s) + A_4 s \cos(\alpha s), \quad (\text{S20})$$

so that

$$\begin{aligned} y'(s) = & A_1 \alpha \cos(\alpha s) + A_2 (\sin(\alpha s) + \alpha s \cos(\alpha s)) \\ & - A_3 \alpha \sin(\alpha s) + A_4 (\cos(\alpha s) - \alpha s \sin(\alpha s)) \end{aligned} \quad (\text{S21})$$

Substitution of Eqs. (S20) and (S21) into the boundary conditions (S13), yields

$$\begin{aligned}
A_3 &= 0 \\
A_1\alpha + A_4 &= 0 \\
A_1\sin(\alpha) + A_2\sin(\alpha) + A_3\cos(\alpha) + A_4\cos(\alpha) &= 0 \\
A_1\alpha\cos(\alpha) + A_2(\sin(\alpha) + \alpha\cos(\alpha)) & \\
-A_3\alpha\sin(\alpha) + A_4(\cos(\alpha) - \alpha\sin(\alpha)) &= 0
\end{aligned} \tag{S22}$$

which admit only trivial solution $\mathbf{a} = \mathbf{0}$, since f in this case has a fixed value (i.e. $f = 2\sqrt{k}$) and cannot vary.

3. For $f^2 - 4k < 0$, Eq. (S14) has four complex roots

$$\alpha = \pi k^{1/4} (\pm \cos \theta \pm i \sin \theta), \tag{S23}$$

where

$$\theta = \frac{1}{2} \left[\pi - \arcsin \left(\sqrt{1 - \frac{f^2}{4k}} \right) \right] \tag{S24}$$

. Therefore, the general solution of Eq. (S6) has the form

$$\begin{aligned}
y(s) = & A_1 \exp(\gamma s) \sin(\beta s) + A_2 \exp(\gamma s) \cos(\beta s) \\
& + A_3 \exp(-\gamma s) \sin(\beta s) + A_4 \exp(-\gamma s) \cos(\beta s),
\end{aligned} \tag{S25}$$

so that

$$\begin{aligned}
y'(s) = & A_1 \exp(\gamma s) (\gamma \sin(\beta s) + \beta \cos(\beta s)) + A_2 \exp(\gamma s) (\gamma \cos(\beta s) - \beta \sin(\beta s)) \\
& + A_3 \exp(-\gamma s) (-\gamma \sin(\beta s) + \beta \cos(\beta s)) - A_4 \exp(-\gamma s) (\gamma \cos(\beta s) + \beta \sin(\beta s)),
\end{aligned} \tag{S26}$$

where $\gamma = \pi k^{1/4} \cos \theta$ and $\beta = \pi k^{1/4} \sin \theta$. Finally, the boundary conditions require that

$$\begin{aligned}
A_2 + A_4 &= 0 \\
A_1\beta + A_2\gamma + A_3\beta - A_4\gamma &= 0 \\
A_1 \exp(\gamma) \sin(\beta) + A_2 \exp(\gamma) \cos(\beta) + & \\
A_3 \exp(-\gamma) \sin(\beta) + A_4 \exp(-\gamma) \cos(\beta) &= 0 \\
A_1 \exp(\gamma) (\gamma \sin(\beta) + \beta \cos(\beta)) + A_2 \exp(\gamma) (\gamma \cos(\beta) - \beta \sin(\beta)) & \\
+ A_3 \exp(-\gamma) (-\gamma \sin(\beta) + \beta \cos(\beta)) + A_4 \exp(-\gamma) (-\gamma \cos(\beta) - \beta \sin(\beta)) &= 0,
\end{aligned} \tag{S27}$$

which can be rewritten as $\mathbf{Ka} = \mathbf{0}$, and the non-zero solution, if exists, is detected by setting $\det(\mathbf{K}) = 0$.

S4 Winkler foundation model: Relation between the spring stiffness K and the matrix shear modulus G_m

In our analysis we adopted the Winkler foundation model and simplified the matrix as an array of springs with stiffness K acting only in radial direction. Therefore, to make a connection between the prediction of the analytical model and the experimental results a relation between the spring stiffness K and the matrix shear modulus $G_m = E_m/[2(1 + \nu_m)]$ needs to be established. For an elastic rod of radius r_r and length L_r buckled into mode n it has been shown that K is related to G_m and ν_m as [8, 9]

$$K = \frac{16\pi G_m (1 - \nu_m)}{2(3 - 4\nu_m) K_0 \left(n\pi \frac{r_r}{L_r} \right) + n\pi \frac{r_r}{L_r} K_1 \left(n\pi \frac{r_r}{L_r} \right)}, \tag{S28}$$

where $K_0(\cdot)$ and $K_1(\cdot)$ are the modified bessel function of second kind.

It is worth noting that for slender rods, for which $r_r/L_r \rightarrow 0$, Eq. (S28) significantly simplifies, since

$$\lim_{r_r/L_r \rightarrow 0} n\pi \frac{r_r}{L_r} K_1 \left(n\pi \frac{r_r}{L_r} \right) = 1 \quad (\text{S29})$$

and

$$\lim_{r_r/L_r \rightarrow 0} K_0 \left(n\pi \frac{r_r}{L_r} \right) = +\infty. \quad (\text{S30})$$

Therefore, when $r_r/L_r \rightarrow 0$ the second term of the denominator in Eq. (S28) can be neglected, so that

$$K = \frac{16\pi G_m (1 - \nu_m)}{2(3 - 4\nu_m) K_0 \left(n\pi \frac{r_r}{L_r} \right)}, \quad (\text{S31})$$

Furthermore, we note that for slender rods

$$\lim_{r_r/L_r \rightarrow 0} \frac{\ln \left(\frac{2L_r}{n r_r} \right)}{K_0 \left(n\pi \frac{r_r}{L_r} \right)} = 1, \quad (\text{S32})$$

and

$$\lim_{r_r/L_r \rightarrow 0} \ln \left(\frac{2L_r}{n r_r} \right) - K_0 \left(n\pi \frac{r_r}{L_r} \right) = 1.72195, \quad (\text{S33})$$

so that Eq. (S31) can be rewritten as

$$K = \frac{16\pi G_m (1 - \nu_m)}{2(3 - 4\nu_m) \ln \left(\frac{2L_r}{n r_r} \right)} \quad \text{when } r_r/L_r \rightarrow 0. \quad (\text{S34})$$

Finally, for the case of rods embedded in soft, elastomeric matrices $\nu_m = 0.5$, so that

$$K = \frac{4\pi G_m}{\ln \left(\frac{2L_r}{n r_r} \right)} \quad \text{when } r_r/L_r \rightarrow 0, \quad (\text{S35})$$

which has been recently used to study buckling of confined microtubules [10].

S5 Relation between λ , K and G_m from Eq. (6)

Although both Eqs. (S28) and (S35) (corresponding to Eqs. (6) and (7) in the main text) indicate that the spring stiffness K depends not only on shear modulus of the matrix G_m , but also on the mode wavelength, $\lambda = 2L_r/n$, in the main text we showed for Eq. (7) that a unique relation between λ , G_m and K can be established by calculating the mode number that minimize the critical force f_n (i.e. calculating n for which $\partial f_n / \partial n = 0$). A similar procedure can be followed to determine the relation between λ , G_m and K also when Eq. (6) is used:

1. Eq. (6) is substituted into Eq. (3), yielding

$$f_n = n^2 + \frac{k}{n^2} = n^2 + \frac{E_m L_r^4}{E_r I_r} \cdot \frac{8}{3\pi^3} \cdot \frac{1}{n^2 (2K_0(n\pi r_r/L_r) + n\pi r_r/L_r \cdot K_1(n\pi r_r/L_r))}, \quad (\text{S36})$$

where, for the sake of simplicity, we assume $\nu_m = 0.5$.

2. The mode number that minimize the critical force f_n is calculated by requiring $\partial f_n / \partial n = 0$,

$$2n - \frac{E_m L_r^4}{E_r I_r} \frac{8}{3\pi^3} \frac{n(2K'_0 \pi r_r / L_r + \pi r_r / L_r K_1 + n \pi r_r / L_r K'_1 \pi r_r / L_r) + 2(2K_0 + n \pi r_r / L_r K_1)}{n^3 (2K_0 + n \pi r_r / L_r K_1)^2} = 0, \quad (\text{S37})$$

where $K_0 = K_0(n \pi r_r / L_r)$ and $K_1 = K_1(n \pi r_r / L_r)$. Note that $n = 2L_r / \lambda$, so that Eq. (S37) can be rewritten in terms of λ as

$$\left(\frac{L_r}{\lambda}\right)^4 \frac{(K_0 + \pi r_r / \lambda \cdot K_1)^2}{L_r / r_r (2K'_0 \pi r_r / L_r + K_1 \pi r_r / L_r + 2\pi r_r / \lambda \cdot K'_1 \cdot \pi r_r / L_r) + (2K_0 + 2\pi r_r / \lambda \cdot K_1)} = \frac{1}{24\pi^3} \frac{E_m L_r^4}{E_r I_r}, \quad (\text{S38})$$

3. The wavelength λ is solved numerically from Eq. (S38);

4. Eq. (6) now provides a unique relation between K and G_m , since λ is known.

S6 An alternative approach for the buckling analysis: the energy approach

In the main text, we used the Winkler foundation model to study analytically the stability of a thin and stiff beam supported by a softer elastic substrate. Following this approach, the interaction between the rod and substrate is simplified as an array of springs with stiffness K acting solely in radial direction, so that the differential equation governing the problem can be easily established and directly solved. However, it is important to highlight the fact the stability analysis can be alternatively conducted by minimizing the total elastic energy of the system [11, 12, 13, 14]. In the following, we study the stability of a rod embedded in a softer matrix using the energy approach and demonstrate that this analysis yields the same results presented in the main text.

We start by constructing the total elastic energy of the system (per unit length), Π_{tot} ,

$$\Pi_{tot} = U_{bending} + U_{stretching} + U_{interaction}, \quad (\text{S39})$$

where $U_{bending}$ and $U_{stretching}$ are the bending and stretching energy per unit length of the rod, respectively, and $U_{interaction}$ denotes the interaction energy between the substrate and the matrix energy per unit length. As typically done [11, 12, 13, 14], we choose the von Karman formulation to describe $U_{bending}$ and $U_{stretching}$. Therefore, denoting with ϵ the applied compressive strain and assuming the buckling mode to be described by a sinusoidal curve, $w = A \sin(n\pi x / L_r)$, we get

$$U_{bending} = \frac{1}{2L_r} E_r I_r \int_0^{L_r} (w'')^2 dx = \frac{1}{4} E_r I_r A^2 \left(\frac{n\pi}{L_r}\right)^4, \quad (\text{S40})$$

$$U_{stretching} = \frac{1}{2L_r} E_r S_r \int_0^{L_r} \left[u' + \frac{1}{2}(w')^2\right]^2 dx = \frac{1}{2} E_r S_r \left[-\epsilon + \frac{1}{4} A^2 \left(\frac{n\pi}{L_r}\right)^2\right]^2, \quad (\text{S41})$$

where S_r is the cross-sectional area of the rod and u and w denote the axial and lateral components of its displacement, respectively.

Finally, we need to specify a form for the interaction energy between the rod and the matrix. Here, as for the Winkler foundation model, we simplified the matrix as an array of springs with

stiffness K acting solely in radial direction, so that

$$U_{interaction} = \frac{1}{2L_r} \int_0^{L_r} K w^2 dx = \frac{1}{4} K A^2. \quad (\text{S42})$$

Note that the spring constant K is not an arbitrary constant. In fact, rigorous expressions for K have been established by modeling the matrix as infinite elastic solid, using the classic theory of elasticity and accounting for the radius of the rod [8].

To determine the critical force F_{cr} , we now substitute Eqs. (S40), (S41) and (S42) into Eq. (S39), and minimize Π_{tot} with respect to A , obtaining

$$\frac{1}{2} E_r I_r A \left(\frac{n\pi}{L_r} \right)^4 + \frac{1}{2} E_r S_r \left[-\epsilon + \frac{1}{4} A^2 \left(\frac{n\pi}{L_r} \right)^2 \right] A \left(\frac{n\pi}{L_r} \right)^2 + \frac{1}{2} K A = 0, \quad (\text{S43})$$

from which the amplitude of the mode A can be solved as

$$A = \begin{cases} \sqrt{\frac{4L_r^4}{E_r S_r (n\pi)^4} \left[-K - E_r I_r \left(\frac{n\pi}{L_r} \right)^4 + E_r S_r \epsilon \left(\frac{n\pi}{L_r} \right)^2 \right]}, & \text{if } E_r S_r \epsilon \left(\frac{n\pi}{L_r} \right)^2 \geq K + E_r I_r \left(\frac{n\pi}{L_r} \right)^4, \\ 0, & \text{if } E_r S_r \epsilon \left(\frac{n\pi}{L_r} \right)^2 < K + E_r I_r \left(\frac{n\pi}{L_r} \right)^4. \end{cases} \quad (\text{S44})$$

The compressive strain required to trigger the n -th mode, ϵ_n , can be then obtained taking the limit for $A \rightarrow 0$ in (S44), yielding

$$\epsilon_n = \frac{I_r}{S_r} \left(\frac{n\pi}{L_r} \right)^2 + \frac{K}{E_r S_r} \left(\frac{L_r}{n\pi} \right)^2, \quad (\text{S45})$$

so that the force required to trigger the n -th mode is given by

$$F_n = E_r S_r \epsilon_n = E_r I_r \left(\frac{n\pi}{L_r} \right)^2 + K \left(\frac{L_r}{n\pi} \right)^2. \quad (\text{S46})$$

At this point we want to highlight the fact that, when normalized, the expression for the critical force given by Eq. (S46) is identical to that reported in Eq. (4) of the main text, confirming the fact that the stability analysis reported in the main text and the one based on the energy approach are equivalent.

The critical mode can then be determined upon calculation of the mode number n that minimizes F_n (*i.e.* determining the values of n for which $\partial F_n / \partial n = 0$). In particular, minimization of F_n using Eq. (S46) yields,

$$E_r I_r \left(\frac{n\pi}{L_r} \right)^2 - K \left(\frac{L_r}{n\pi} \right)^2 + \frac{1}{2} \frac{\partial K}{\partial n} \frac{L_r}{\pi} = 0, \quad (\text{S47})$$

which reduces to the expression reported in Eq. (9) of the main text when the expression for K provided by Eq. (S35) is substituted in, further demonstrating that the energy approach converges to the exact same results obtained by solving directly the differential equations.

Finally, we want to highlight the fact that, although in literature different forms for the interaction energy $U_{interaction}$ have been used [11, 12, 13, 14], the reported results closely resemble those derived above. To demonstrate this important point, we follow Jiang et al. [13] and

construct $U_{interaction}$ by superposition of a series of solutions for point loads in the (semi-) infinite 3D space ¹, yielding

$$U_{interaction} = \frac{3\beta^2}{32\pi E_m} \left[3 - 2\gamma - 2 \ln \left(\frac{n\pi r_r}{L_r} \right) \right], \quad (S48)$$

where $\gamma = 0.577$ is the Euler's constant and β is given by

$$\beta = -E_r I_r A \left(\frac{n\pi}{L_r} \right)^4 - E_r S_r \left[\frac{1}{4} A^2 \left(\frac{n\pi}{L_r} \right)^2 - \epsilon \right] A \left(\frac{n\pi}{L_r} \right)^2. \quad (S49)$$

Substitution of Eq. (S48) into Eq. (S39), and minimization of Π_{tot} with respect to A results in the following prediction for the wave number n (see Eq. (32) in [13])

$$n \left(\frac{E_r I_r}{G_m} \right)^{1/4} = \left\{ \frac{16\pi [1 - \gamma - \ln(n r_r)]}{[3 - 2\gamma - 2 \ln(n r_r)]^2} \right\}^{1/4}, \quad (S50)$$

where $G_m = E_m / (2(1 + \nu_m))$ is the initial shear modulus of the matrix. Noting for an incompressible matrix (i.e. $\nu_m = 0.5$)

$$G_m = \frac{E_m}{3}, \quad (S51)$$

and that

$$\ln(n r_r) = \ln(2\pi) - \ln(\lambda/r_r), \quad (S52)$$

$\lambda = 2\pi/n$ being the wavelength, Eq. (S50) can be rewritten as

$$\frac{(\lambda/L_r)^4 [\ln(\lambda/r_r) + 1 - \gamma - \ln(2\pi)]}{[2 \ln(\lambda/r_r) + 3 - 2\gamma - 2 \ln(2\pi)]^2} = \frac{3\pi^3}{\eta}, \quad (S53)$$

where $\eta = (E_m L_r^4) / (E_r I_r)$ is the dimensionless matrix stiffness. Furthermore, as noted by the authors in [13], for a wide range of values of E_m Eq. (S53) can be simplified to

$$\frac{\lambda}{L_r} = 3^{1/4} \cdot 8\pi/5 \cdot \eta^{-1/4} = 6.62\eta^{-1/4}. \quad (S54)$$

The equation above has exactly the same structure as Eq. (10) in the main text

$$\frac{\lambda}{L_r} = \alpha \eta^{-1/4}, \quad (S55)$$

where the prefactor α is found to lie within $6.71 < \alpha < 7.04$ depending on the values of λ/r_r . Finally, it is worth noting that if we take the limit for $\lambda/r_r \rightarrow +\infty$, Eq. (S53) and Eq. (9) in the main text yield exactly the same expression for the wavelength λ .

S7 Discrete elastic rod simulations

In Tab. S2 we summarize all parameters used in the 22 discrete elastic rod simulations we performed and the corresponding results. In all the simulations we considered a rod with length $L_r = 9.7\text{cm}$, diameter $d_r = 100\mu\text{m}$, density $\rho = 6500\text{kg/m}^3$, Young's modulus $E_r = 64.24\text{GPa}$ and Poisson's ratio $\nu = 0.5$. We discretized the rod into 203 segments with $nv = 204$ nodes. The simulations were performed with control displacement boundary conditions, where one end of the rod was pinned and the other end was displaced at a constant rate of $v_p = 0.05\text{mm/s}$.

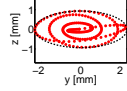
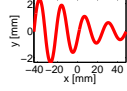
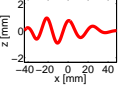
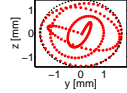
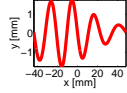
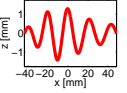
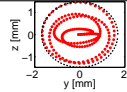
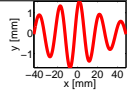
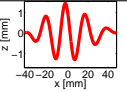
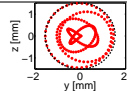
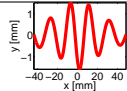
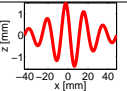
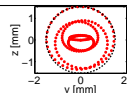
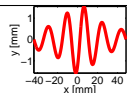
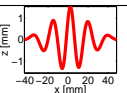
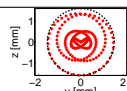
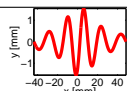
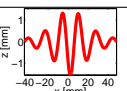
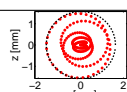
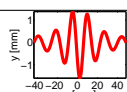
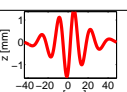
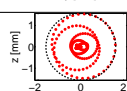
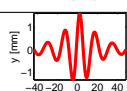
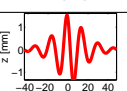
¹Note that the interaction energy constructed in this way does not account for the radius of the rod.

Table S2: BASim parameters and results. For each simulation, the dimensionless contact spring constant k_{dim} , the predicted buckling mode, the measured b/a for the minimum area ellipse, and also the buckled configurations are reported.

| Simulation Parameters | | | | | | |
|--|------------------|-------------|---------------------------|--------------------|-------------|-------------|
| $\rho = 6500\text{kg/m}^3$; $L_r = 9.7\text{cm}$; $d_r = 100\mu\text{m}$; $E_r = 64.24\text{GPa}$; $G_r = 21.41\text{GPa}$; $\nu = 0.5$; $nv=204$; $v_p = 0.05\text{mm/s}$. | | | | | | |
| ID | k_{dim} | mode number | b/a at $\epsilon = 5\%$ | Cross-section view | Side view 1 | Side view 2 |
| 1 | 400 | 4/5 | 0.13 | | | |
| 2 | 525 | 5 | 0.00 | | | |
| 3 | 650 | 5 | 0.00 | | | |
| 4 | 775 | 5 | 0.00 | | | |
| 5 | 900 | 5/6 | 0.30 | | | |
| 6 | 1116 | 6 | 0.03 | | | |
| 7 | 1332 | 6 | 0.00 | | | |
| 8 | 1548 | 6 | 0.03 | | | |
| 9 | 1764 | 6/7 | 0.34 | | | |
| 10 | 2107 | 7 | 0.39 | | | |
| 11 | 2450 | 7 | 0.05 | | | |
| 12 | 2793 | 7 | 0.23 | | | |
| 13 | 3136 | 7/8 | 0.53 | | | |
| 14 | 3648 | 8 | 0.59 | | | |

Simulation Parameters

$\rho = 6500\text{kg/m}^3$; $L_r = 9.7\text{cm}$; $d_r = 100\mu\text{m}$; $E_r = 64.24\text{GPa}$; $G_r = 21.41\text{GPa}$; $\nu = 0.5$;
 $nv=204$; $v_p = 0.05\text{mm/s}$.

| ID | k_{dim} | mode number | b/a at $\epsilon = 5\%$ | Cross-section view | Side view 1 | Side view 2 |
|----|------------------|-------------|---------------------------|---|---|---|
| 15 | 4160 | 8 | 0.40 |  |  |  |
| 16 | 5184 | 8/9 | 0.82 |  |  |  |
| 17 | 6642 | 9 | 0.86 |  |  |  |
| 18 | 8100 | 9/10 | 0.94 |  |  |  |
| 19 | 10100 | 10 | 0.97 |  |  |  |
| 20 | 12100 | 10/11 | 1.00 |  |  |  |
| 21 | 14762 | 11 | 0.97 |  |  |  |
| 22 | 17424 | 11/12 | 0.96 |  |  |  |

References

- [1] A. N. Gent, *Engineering with Rubber: How to Design Rubber Components*, Hanser Publications, 2nd ed., 2001.
- [2] F. Brau, H. Vandeparre, A. Sabbah, C. Poulard, A. Boudaoud and P. Damman, Multiple-length-scale elastic instability mimics parametric resonance of nonlinear oscillators, *Nat. Phys.*, 2011, **7**, 56-60.
- [3] J. Nase, Debonding of viscoelastic materials: From a viscous liquid to a soft elastic solid, Ph.D. thesis, Universität des Saarlandes and Université Pierre et Marie Curie, 2009.
- [4] X. Q. Brown, K. Ookawa, and J. Y. Wong, Evaluation of polydimethylsiloxane scaffolds with physiologically-relevant elastic moduli: interplay of substrate mechanics and surface chemistry effects on vascular smooth muscle cell response, *Biomaterials*, 2005, **26**, 3123-3129.
- [5] D. S. Gray, J. Tien, and C. S. Chen, Repositioning of cells by mechanotaxis on surfaces with micropatterned young's modulus, *J. Biomed. Mater. Res. A.*, 2003, **66**, 605-614.
- [6] I. T. Jolliffe, *Principal Component Analysis*, Springer, 2nd ed., 2002.
- [7] M. Ringnér, What is principal component analysis? *Nat. Biotechnol.*, 2008, **26**, 303-304.
- [8] L. R. Herrmann, W. E. Mason and S. T. K. Chan, Response of reinforcing wires to compressive states of stress, *J. Compos. Mater.*, 1967, **1**, 212-226.
- [9] Y. Lanir and Y. C. B. Fung, Fiber composite columns under compression, *J. Compos. Mater.*, 1972, **6**, 387-401.
- [10] C. P. Brangwynne, F. C. MacKintosh, S. Kumar, N. A. Geisse, J. Talbot, L. Mahadevan, K. K. Parker, D. E. Ingber and D. A. Weitz, Microtubules can bear enhanced compressive loads in living cells because of lateral reinforcement, *J. Cell Biol.*, 2006, **173**, 733-741.
- [11] Wu J, Liu ZJ, Song J, Huang Y, Hwang KC, Zhang YW, Roger JA, Stretchability of encapsulated electronics, *Appl. Phys. Lett.*, 2011, **99**, 061911.
- [12] Jiang H, Sun Y, Rogers JA, Huang Y, Post-buckling analysis for the precisely controlled buckling of thin film encapsulated by elastomeric substrates, *Int. J. Solids. Struct.*, 2008, **45**, 2014-2023.
- [13] Jiang H, Zhang J, Mechanics of microtubule buckling supported by cytoplasm, *J. Appl. Mech.*, 2008, **75**, 061019.
- [14] Huang ZY, Hong W, Suo Z, Nonlinear analyses of wrinkles in a film bonded to a compliant substrate, *J. Mech. Phys. Solids.*, 2008, **53**, 2101-2118.